Electronic Supplementary Information

Hierarchical $Zn_2Mo_3O_8$ nanodots-porous carbon composite as a superior anode for lithium-ion batteries

Yanping Zhu[a, b, c], Yijun Zhong[a, b, c], Gao Chen[a, b, c], Xiang Deng[a, b, c], Rui Cai[a, c], Li Li[d], Zongping Shao[a, b, d, e]*

[a] *Jiangsu National synergetic Innovation Center for Advanced Materials*

[b] *State Key Laboratory of Materials-Oriented Chemical Engineering, Nanjing Tech University, Nanjing 210009, China*

[c] *College of Chemistry & Chemical Engineering, Nanjing Tech University, Nanjing 210009, China*

[d] *College of Energy, Nanjing Tech University, Nanjing 210009, China*

[e] *Department of Chemical Engineering, Curtin University, Perth, WA 6845, Australia*

Experimental

2.1 Material synthesis

All the chemicals employed in this work were analytical regents without further purification. In a typical synthesis process of the $Zn_2Mo_3O_8$-C composite, the pretreated macroporous cinamic anion-exchange resin (D201) (10 g) was firstly immersed into 0.075 mol L^{-1} of ammonium molybdate tetrahydrate (AHM) aqueous solution (100 mL) and stirred magnetically for 10 h at room temperature (RT). The adsorbed resin was collected after rinsing, drying and grinding. Then 2 g of the adsorbed resin powder was added into 100 mL of zinc chloride ($ZnCl_2$)-ethanol solution containing 10 g of $ZnCl_2$ under vigorously stirring at 70 ^oC in oil bath for 10 h to allow the ethanol to evaporate slowly. Finally, the above paste-like adsorbed resin-$ZnCl_2$ mixture was transferred to a quartz boat and pre-treated at 150 ^oC for 3 h in argon to remove moisture, and then, the furnace temperature rose from 150 ^oC to 600 ^oC and held for 2 h (ramp rate: 2 ^oC min^{-1}). After cooling naturally to RT, the product was introduced into 1 M hydrochloric acid solution and stirred for 6 h at RT. The ZMO/PC composite was subsequently obtained by repeat washing with deionized water and vacuum desiccated at 60 ^oC for 12 h. As control experiments, the $ZnCl_2$ activated carbon was prepared following the same procedure without the addition of AHM and denoted as "$ZnCl_2$–C"; the sample without the attendance of $ZnCl_2$ is named "Mo-C".

2.2 Characterization

The crystallographic information of the samples were evaluated through RT powder X-ray diffraction (XRD) measurement on a Bruker D8 Advance diffractometer with Cu Kα source over a 2θ range from 20° to 80°. The microstructure images were observed with field-emission scanning electron microscope (FE-SEM) (HITACHI S-4800), transmission electron microscope (TEM) and high-resolution transmission electron microscope (HR-TEM) (JEOL JEM-200CX). X-ray photoelectron spectroscopy (XPS) analysis was carried out using a PHI550 system and the as-obtained spectra were fitted through XPSPEAK41 software. Raman spectra

were collected by an HR800 UV micro-Raman spectrometer. Thermogravimetric analysis (TGA) was performed employing a WCT-1 TG Analyzer under air flow to determine the carbon content of the product. Nitrogen adsorption-desorption isotherms were measured using an adsorption-desorption instrument (BELSORP-MINI, Japan) with nitrogen at 77 K. The samples were pretreated at 200 °C for 2 h under vacuum to remove surface-adsorbed species before analysis. Specific surface area of the samples was calculated using the Brunauer-Emmett-Teller (BET) equation. Pore-size distributions (PSD) were calculated from the adsorption branch of the isotherm using QSDFT method.

2.3 Electrode fabrication and electrochemical measurements

The working electrodes were comprised of electroactive materials (ZMO/PC or PC), conductive agent (Super P) and binder (polyvinylidene fluoride) at a weight ratio of 8:1:1 with solvent (N-methyl-2-pyrrolidone) upon the current collector (Cu foils). The well-mixed anode slurries were carefully deposited on Cu foils and dried at 100 ^{o}C for 12 h in a vacuum oven. Then the obtained electrodes were cut into 14 mm disks for the subsequent step and the loading of active materials ranged from 1 to 1.5 mg. CR2016-type coin cells were assembled by sandwiching the microporous polypropylene membrane (Celgard 2400) between the working electrode and the counter electrode (lithium metal foil, also the reference electrode) in a pure-argon filled glove box where both of the oxygen and moisture content were restricted to less than 0.1 ppm. 1 M $LiPF_6$ in ethylene carbonate (EC) and dimethyl carbonate (DMC) (1: 1, v:v) was used here as liquid electrolyte. All the assembled cells were statically placed for at least 6 h to ensure the sufficient infiltration of electrolyte into the electrodes before electrochemical measurements. RT-galvanostatically discharge/charge cycling performance was conducted over the potential range of 3.00-0.01 V on the NEWARE BTS multichannel battery testing system (5 V, 10 mA). Cyclic voltammetry profiles were acquired from a PARSTAT 273A electrochemical workstation and the scanning rate was set as 0.1 mV s^{-1}. Electrochemical impedance spectroscopy (EIS) was performed with Princeton

2273 electrochemical system at a frequency range of 100 kHz to 0.1 Hz at open circuit voltage (OCV) over the single cell.

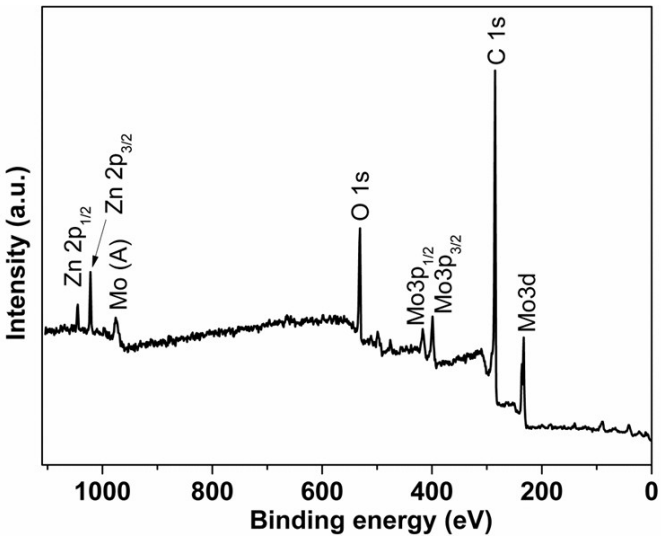

Fig. S1 Survey XPS spectrum of the $Zn_2Mo_3O_8$-C composite.

Table S1. Physical Properties of materials

Sample	$a_{s,BET}$ $m^2\ g^{-1}$	V_{Total} ($P/P_0 = 0.99$) $cm^3\ g^{-1}$
Mo-C	32	0.11
$ZnCl_2$-C	877	0.73
$Zn_2Mo_3O_8$-C	350	0.90
$Zn_2Mo_3O_8$-C@HNO_3	943	1.2

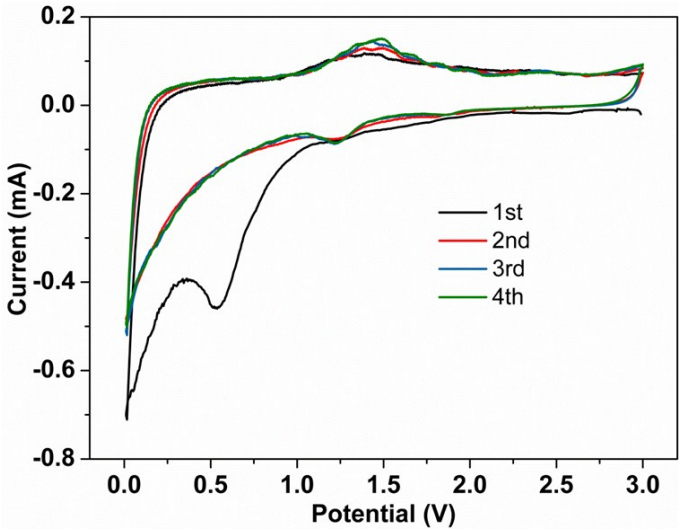

Fig. S2 Cyclic voltammogram of the $Zn_2Mo_3O_8$-C electrode at a scanning rate of 0.1 mV s^{-1}.

Equations 1

$$Zn_2Mo_3O_8 + 16Li^+ + 16e^- \rightarrow 2Zn + 3Mo + 8Li_2O$$

Equations 2

$$2Zn + 2Li^+ + 2e^- \leftrightarrow 2LiZn$$

Equations 3

$$2Zn + 2Li_2O \leftrightarrow 2ZnO + 4Li^+ + 4e^-$$

Equations 4

$$3Mo + 6Li_2O \leftrightarrow 3MoO_2 + 12Li^+ + 12e^-$$

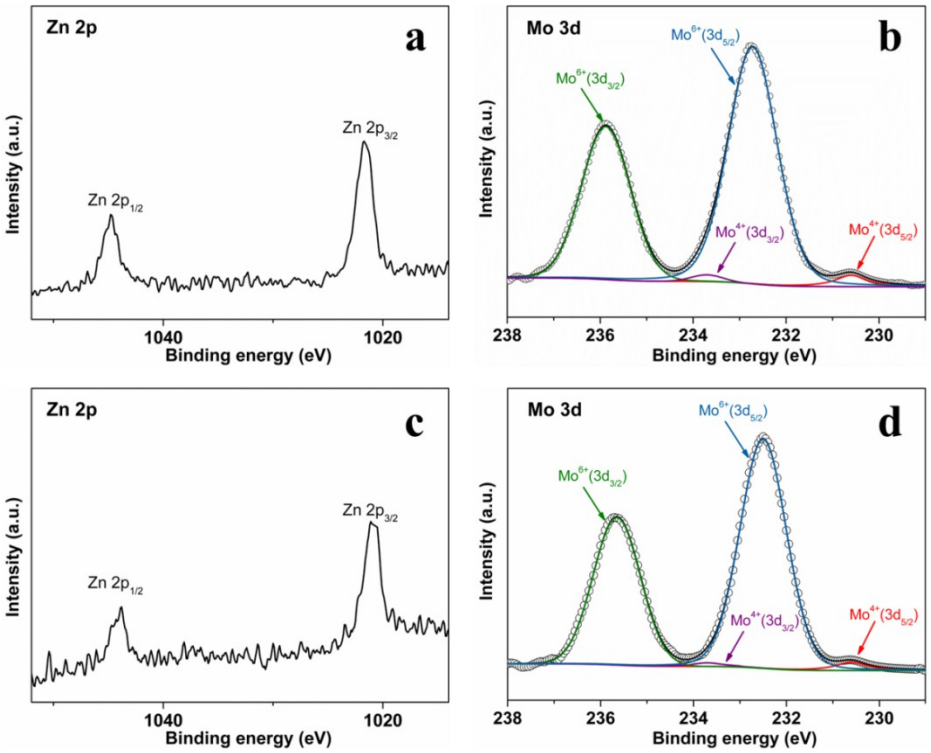

Fig. S3 High-resolution XPS spectra of Zn 2p and Mo 3d of the electrode material (a, b) after the 1st cycle and (c, d) after the 50th cycle.

The electrode materials after different cycles have been investigated by XPS with the results displayed in **Fig. S3**. After the 1st cycle, the high-resolution Zn 2p core level spectrum (**Fig. S3a**) reveals two peaks with binding energies of 1021.6 eV and 1044.7 eV corresponded to Zn $2p_{3/2}$ and Zn $2p_{1/2}$, respectively, which is typically related to the Zn (II) oxidation state.[1] The fitted Mo 3d spectrum in **Fig. S3b** shows peaks located at 230.6 eV for Mo $3d_{5/2}$ and 233.7 eV for Mo $3d_{3/2}$, confirming the Mo (IV) oxidation state. Meanwhile, the other two peaks positioned at 232.7 eV and 235.8 eV are ascribed to Mo (VI) $3d_{5/2}$ and Mo (VI) $3d_{3/2}$, respectively, probably due to the oxidation of surface Mo (IV) during the sample preparation for XPS characterization.[2] Chowdari *et al* [3] analyzed the similar case of $Co_2Mo_3O_8$, and the formation of MoO_2 is favorable after charge process. So the formation of MoO_2 after cycle is well confirmed. After the 50th cycle, likewise, the valence of Zn and Mo element remains the same, as suggested by the high-resolution Zn 2p and Mo 3d XPS spectrum in **Fig. S3c&S3d**.

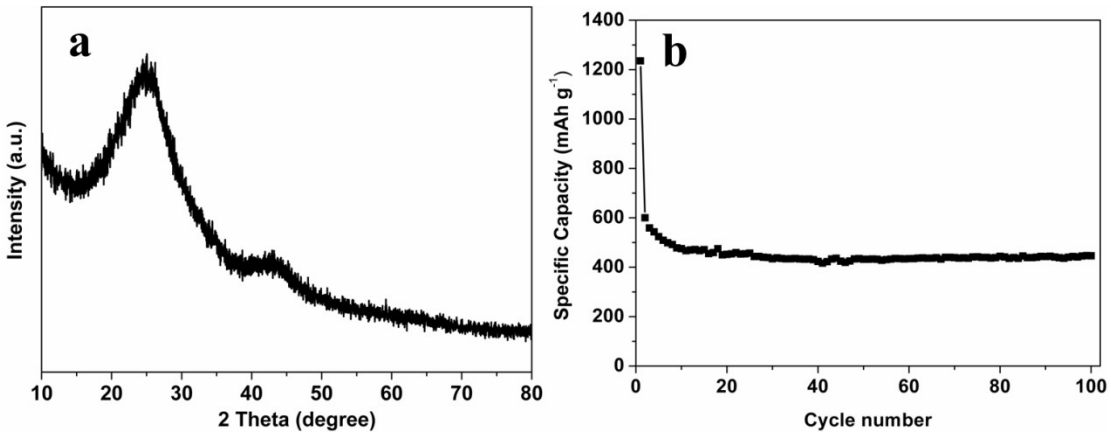

Fig. S4 (a) XRD pattern of the $ZnCl_2$-C. (b) Cycling performance of $ZnCl_2$-C electrodes at a current density of 0.2 A g^{-1}.

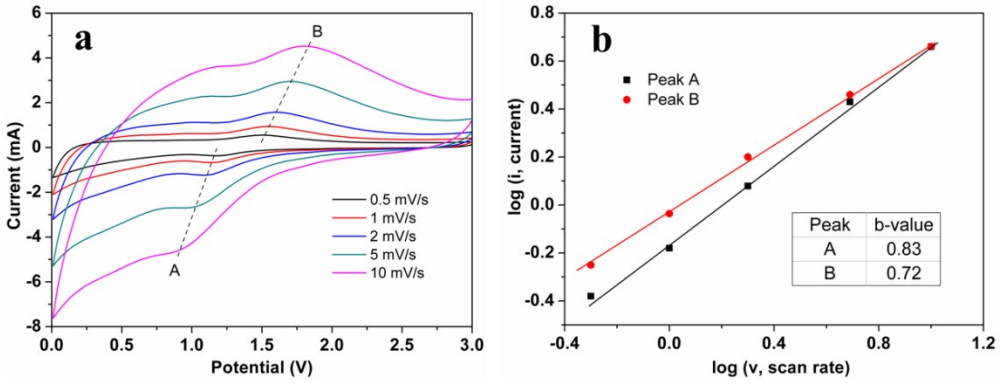

Fig. S5 (a) CV curves at different scan rates and (b) log *i vs* log *v* plots for cathodic and anodic sweeps of CV.

The theoretical specific capacity of neat $Zn_2Mo_3O_8$ was calculated on the basis of 16 Li^+ insertion/extraction, and it turned out to be **883 mA h g^{-1}**. The as-synthesized $Zn_2Mo_3O_8$-C composite displays a reversible specific capacity of 953 mA h g^{-1}, which is much higher than the theoretical value for the composite ($C_{theoretical} = C_{Zn2Mo3O8} \times$ mass percentage of $Zn_2Mo_3O_8 + C_{carbon} \times$ mass percentage of C = 883 × 52% + 450 × 48% = **675 mA h g^{-1}**). For the nanosized particles, both capacitive and lithium intercalation processes contribute to the total capacity.[4] In order to explain the high performance of the $Zn_2Mo_3O_8$-C electrode, the capacitive effect of the battery system is calculated by analyzing the cyclic voltammetry data at various sweep rates

according to Equations (1) and (2):

$$i = a\, v^b \quad (1)$$

$$\log i = b \times \log v + \log a \quad (2)$$

Where i is the current density, v is the scan rate, and a and b are adjustable parameters. For a typical Li^+ diffusion controlled process, b is 0.5, while for ideal capacitive behavior, b is 1. **Fig. S5a** shows the CV profiles of the $Zn_2Mo_3O_8$-C at different sweep rates. Two peaks, marked as A and B, appear during the cathodic (discharge) and anodic (charge) process. In the log i *vs* log v plots (**Fig. S5b**), the b values can be determined as 0.83 and 0.72 for peak A and peak B, respectively. The b-values are both greater than 0.5, indicating the pseudocapacitive effect of the $Zn_2Mo_3O_8$-C. It means that a combination of capacitive process and diffusion-limited redox reaction manage the electrochemical reaction, which is beneficial for improving the specific capacity, as well as cycling life and rate capability in LIBs. In addition, the decomposition of electrolyte and formation of electrochemically active polymeric gel-like film on the surface of the electrodes can also contributed to the extra capacity.[5]

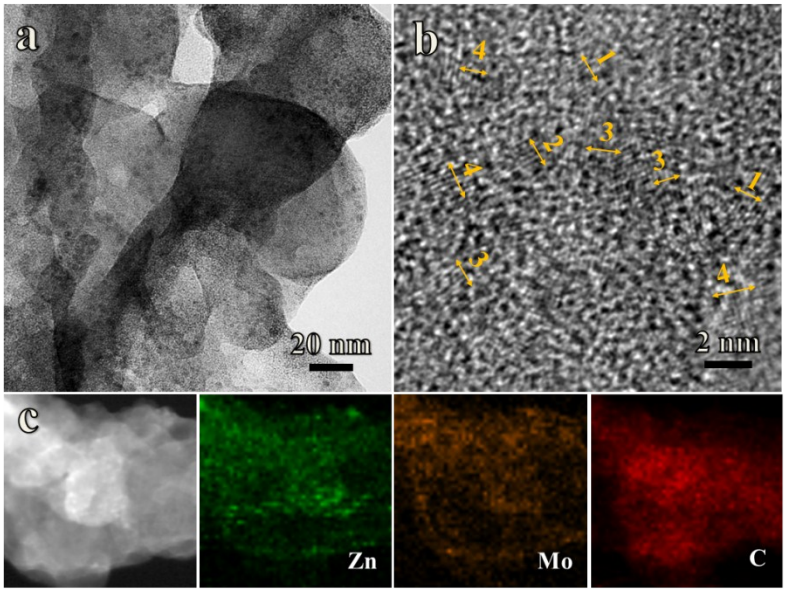

Fig. S6 Ex-situ (a) TEM, (b) HRTEM images of the charged $Zn_2Mo_3O_8$-C electrode at 3.0 V after 210 discharge-charge cycles and (c) S-TEM image and the corresponding elemental mapping images of zinc, molybdenum, carbon.

Table S2 Comparison of the interplanar spacings derived from HRTEM image (**Fig. S6b)** with the literature data on ZnO and MoO_2.

Number	d [Å]	ZnO (JCPDS-80-0074) d[Å] (hkl)	MoO_2 (JCPDS-78-1072) d[Å] (hkl)
1	1.63	1.627 (110)	
2	1.91	1.913 (102)	
3	2.43		2.430 (020)
4	2.19		2.192 (-212)

References

1 L. R. Hou, H. Hua, L. Lian, H. Cao, S. Q. Zhu and C. Z. Yuan, *Chem. Eur. J.* 2015, **21**, 13012-13019.

2 X. Wang, Y. Xiao, J. Q. Wang, L. N. Sun and M. H. Cao, *J. Power Sources*, 2015, **274**, 142-148.

3 B. Das, M. V. Reddy, S. Tripathy and B. V. R. Chowdari, *RSC Adv.*, 2014, **4**, 33883-33889.

4 (a) L. C. Yang, W. Sun, Z. W. Zhong, J. W. Liu, Q. S. Gao, R. Z. Hu and M. Zhu, *J. Power Sources*, 2016, **306**, 78-84; (b) B. T. Zhao and Z. P. Shao, *J. Phys. Chem. C*, 2012, **116**, 17440-17447.

5 A. Bhaskar, M. Deepa and T. N. Rao, *ACS Appl. Mater. Interfaces*, 2013, **5**, 2555-2566.